Electronic and crystal structures of $(Na_{1-x}Ca_x)Cr_2O_4$ with anomalous colossal magnetoresistance

Hitoshi Yamaoka,[1,*] Eike F. Schwier,[2,†] Yoshiya Yamamoto,[3,‡] Masashi Nakatake,[2,§] Masahiro Sawada,[2] Hiroya Sakurai,[4] Naohito Tsujii,[5] Masashi Arita,[2] Hideaki Iwasawa,[2,‖] Munetaka Taguchi,[6] Kenya Shimada,[2] and Jun'ichiro Mizuki[3]

[1]*RIKEN SPring-8 Center, Sayo, Hyogo 679-5148, Japan*

[2]*Hiroshima Synchrotron Radiation Center, Hiroshima University, Higashi-Hiroshima, Hiroshima 739-0046, Japan*

[3]*Graduate School of Science and Technology, Kwansei Gakuin University, Sanda, Hyogo 669-1337, Japan*

[4]*National Institute for Materials Science, 1-1 Namiki, Tsukuba, Ibaraki 305-0044, Japan*

[5]*International Center for Materials Nanoarchitectonics, National Institute for Materials Science, Sengen 1-2-1, Tsukuba 305-0047, Japan*

[6]*Toshiba Nanoanalysis Corporation Kawasaki, Kanagawa 212-8583, Japan*

(Received 9 August 2020; revised 14 November 2020; accepted 7 December 2020; published 23 December 2020)

The electronic and crystal structures of $(Na_{1-x}Ca_x)Cr_2O_4$ have been studied in detail by combining photoelectron spectroscopy (PES), x-ray absorption spectroscopy (XAS), and x-ray diffraction (XRD). The PES results suggest a gap opening at the Fermi level with decreasing temperature and/or increasing the Ca concentration. The XAS spectra at the O K-absorption edge suggest a slight increase of the O $2p$–Cr $3d$ hybridization at low temperatures in $NaCr_2O_4$ and $Na_{0.8}Ca_{0.2}Cr_2O_4$, which corresponds to the appearance of the antiferromagnetic order. However, XRD showed no corresponding structural transition. The experimental results were compared with spin-resolved density functional theory (DFT) calculations. In $Na_{1-x}Ca_xCr_2O_4$ the pre-edge intensity of the XAS spectra at the O K-absorption edge is strongly suppressed with increasing x, in accordance with the gap opening by Ca doping. This observation is consistent with the DFT calculation, where the density of states just above and below the Fermi level diminishes as the electron is doped into $NaCr_2O_4$.

DOI: 10.1103/PhysRevB.102.235150

I. INTRODUCTION

$NaCr_2O_4$ shows unconventional colossal magnetoresistance (CMR) below antiferromagnetic (AFM) ordering temperature of $T_N = 125$ K [1,2]. It has calcium ferrite type structure, where one-dimensional electronic correlations and geometrical frustrations can coexist [1]. Electrical resistivity of $NaCr_2O_4$ diverges with decreasing temperature without magnetic field, indicating insulating behavior. While the resistivity is largely decreased under magnetic field, the CMR effect is progressively enhanced with decreasing temperature with no thermal or field hysteresis. The conventional CMR effect appears only around ferromagnetic transition temperature and has been considered to be originated by the suppression of thermal fluctuation of the ferromagnetic moment by magnetic field. Therefore, CMR becomes smaller normally with decreasing temperature and the resistivity is significantly low at low temperatures even without magnetic field. Another interesting feature is that $NaCr_2O_4$ does not show hysteresis induced by temperature or magnetic field. Thus, the CMR of $NaCr_2O_4$ is anomalous.

$NaCr_2O_4$ does not show the structural transition associated with the metal-to-insulator transition (MIT) as seen in VO_2 [3–5], V_2O_3 [4], $K_2Cr_8O_{16}$ [6,7]. A sister compound, vanadium oxide NaV_2O_4, takes a quasi-one-dimensional metallic ground state even at low temperatures [8], which is different from $NaCr_2O_4$, while the valence band spectra of NaV_2O_4 [9] are very similar to those of $NaCr_2O_4$. NaV_2O_4 is a mixed-valent $V^{3.5}$ ($3d^{1.5}$) compound consisting of double chains of edge-sharing VO_6.

Usually, early transition metal oxides with low valence state belong to the insulator of Mott-Hubbard type. As the valence of the transition metal increased and/or the d level is lowered, the system may enter to the regime of small or negative Δ. Nuclear magnetic resonance (NMR) study for $NaCr_2O_4$ showed no charge ordering of Cr^{3+} and Cr^{4+}, but the mixed valence state of $Cr^{3.5}$ [10]. In $(Na_{1-x}Ca_x)Cr_2O_4$ recent x-ray absorption spectroscopy (XAS) study at the O K-absorption edge showed the holes on the oxygen ions and mixed valence state of $NaCr_2O_4$ [11,12]. Taguchi *et al.* suggested an unusual coexistence of negative and positive charge transfer in mixed valent $Na_xCa_{1-x}Cr_2O_4$ [12]. Ca substitution to the Na site changed the Cr valence from 3.5 for $NaCr_2O_4$ to 3 for $CaCr_2O_4$. In $(Na_{1-x}Ca_x)Cr_2O_4$, T_N rapidly decreased with increase of Ca content from $x = 0$ to $\frac{1}{3}$ [2]. Spin-glass behavior has been observed for $0.4 \leqslant x \leqslant 0.9$. Zero-field μSR spectra suggested the incommensurate AF order below T_N in β-$CaCr_2O_4$ [13]. The Cr moments in each zigzag chain are aligned ferromagnetically along the c axis, whereas

*Corresponding author: yamaoka@spring8.or.jp

†Corresponding author: schwier@hiroshima-u.ac.jp

‡Present address: Nagoya Institute of Technology, Showa, Nagoya 466-8555, Japan.

§Present address: Aichi Synchrotron Radiation Center, Seto, Aichi 489-0965, Japan.

‖Present address: Synchrotron Radiation Research Center, National Institutes for Quantum and Radiological Science and Technology, Sayo, Hyogo 679-5148, Japan.

antiferromagnetically along the *a* axis between the adjacent zigzag chains [14,15]. Unusual temperature dependence of the spin-flop transition field in magnetic phase diagram of $NaCr_2O_4$ suggested the existence of spin frustrations [14]. Thus, $NaCr_2O_4$ showed very different physical properties compared to other 3*d* oxide compounds.

The electronic structure plays an important role for the unusual physical properties in $NaCr_2O_4$, but no systematic measurement has been reported so far except the chemical composition dependence of XAS spectra at room temperature [11,12]. In this paper, we show a systematic study of the temperature and chemical composition dependencies of the electronic and crystal structures of $(Na_{1-x}Ca_x)Cr_2O_4$ with photoelectron spectroscopy (PES), XAS, and x-ray diffraction (XRD). We also performed the XAS study of the temperature dependencies of the electronic structure under the magnetic field. The purpose of the paper is to clarify the correlation between the electronic and crystal structures and the transport properties such as the resistivity and magnetic order as a function of temperature, Ca doping, and magnetic-field dependencies. The electron doping with the Ca substitution causes large change in the electronic structure above the Fermi level, while the temperature induces a slight change in the electronic structure of the valence and conduction bands. No temperature-induced structural transition was observed for the compounds measured. Spin-resolved density functional theory (DFT) calculation study was performed for $NaCr_2O_4$ and $CaCr_2O_4$. Possible origins to open the gap are discussed. The present experimental and theoretical results suggest that the mechanism of the gap opening with the Ca substitution is different from that with the temperature.

II. METHODS AND MATERIAL PROPERTIES

A. Experiments

$NaCr_2O_4$ was synthesized using a high-pressure and high-temperature technique [1]. $NaCr_2O_4$ has $CaFe_2O_4$-type orthorhombic structure with a space group *Pnma* (No. 62, D_{2h}^{16}), in which Cr_2O_4 double chains, i.e., zigzag chains formed on the *bc* plane by a network of edge-sharing CrO_6 octahedra align along the *b* axis. In the zigzag chain, spin frustration of Cr atoms may occur. β-$CaCr_2O_4$ has the same crystal structure as $NaCr_2O_4$ and identical fractional atomic coordinates, but the slightly different space group (*Pbnm* No. 62cab, D_{2h}^{16}). A powder sample of $NaCr_2O_4$ was synthesized at 7 GPa pressure from a stoichiometric mixture of $NaCrO_2$, Cr_2O_3, and CrO_3. $NaCrO_2$ was prepared from a stoichiometric mixture of Na_2CO_3 and Cr_2O_3 at 850 °C in flowing Ar gas. The dense polycrystalline $NaCr_2O_4$ sample was compressed under a pressure of 7 GPa using a belt-type press, and then kept at 1300 °C for 6 h. After quenching to room temperature, the pressure was gradually reduced to ambient.

The temperature dependence of the resistivity shows that $NaCr_2O_4$ has an anomaly at $T_N = 125$ K [1]. The fit to the Arrhenius plot in the temperature range from 200 to 300 K in $(Na_{1-x}Ca_x)Cr_2O_4$ shows clearly that the Ca substitution also makes the energy gap larger and compounds insulators [16]. The magnetic susceptibility takes maximum around 15%–20% Ca substitution at low temperatures [2]. The magnetic transition is not observed at 40%–90% Ca substitution, but $CaCr_2O_4$ shows incommensurate AF order at $T_N = 21$ K [13].

The temperature dependence of the lattice constants was measured down to 10 K using a Rigaku RINT2000 x-ray diffractometer at RIKEN. Vacuum ultraviolet (VUV) PES was performed at the beamline BL-7, the Hiroshima Synchrotron Radiation Center (HiSOR), equipped with a hemispherical electron-energy analyzer (Gammadata-Scienta SES-2002). In the VUV PES the energy resolution (ΔE) was set to 40–50 meV around $h\nu = 40$ eV under the vacuum pressure below 10^{-8} Pa. Samples were fractured in vacuum just before the measurements. It is noted that the pre-edge intensity of the XAS spectra at the O *K*-absorption edge in the fractured surface was enhanced compare to that in the nonfractured surface. The energy resolution and the Fermi level are determined with a fit of the Fermi edge of Au using a convolution of a Gaussian and a Fermi-Dirac functions. Charge up of the samples was checked by the shift of the core-level spectra. XAS were performed at BL-14 at HiSOR with the total electron yield mode on the fresh sample surface obtained by fracturing in the vacuum [17]. ΔE was set to be on the order of less than 0.1 eV around $h\nu = 540$ eV. XAS under the magnetic field of 1.1 T using a pair of the permanent magnets were also performed.

B. Density functional theory calculations

DFT calculations for $NaCr_2O_4$ and β-$CaCr_2O_4$ were performed using the ELK code, [18] which is based on an all-electron full-potential linear augmented plane wave (FP-LAPW) method. Exchange and correlation energies were described by the revised PBE functional introduced by Zhang and Yang [19] and a 4×12×4 *k* mesh centered around the Γ point was employed to sample the Brillouin zone resulting in 54 nonequivalent *k* points. The muffin-tin radii were set as follows: Na and Ca ($r_{Na} = r_{Ca} = 2.2a_0$), Cr ($r_{Cr} = 2.4a_0$), and O ($r_O = 2.0a_0$). The muffin-tin radii of Ca and O were modified from the standard values ($r_{Ca} = 2.4a_0$ and $r_O = 1.8a_0$, respectively) to allow a direct comparison between the Na and Ca calculation and to reduce the mismatch between the Cr and O muffin-tin radii. Due to the short bond length between Cr and O atoms their muffin-tin radii where further reduced automatically by the DFT code ($r_{Cr} \approx 1.95a_0$ and $r_O \approx 1.62a_0$, respectively). The cutoff parameter *rgkmax* was set to 6.5. Onsite electron correlations were simulated within the DFT + *U* scheme as implemented in the ELK code [20,21]. Double counting was accounted for by self-consistently interpolating between the fully localized limit (FFL) and around mean field (AMF) [22]. No distinction was made between the different crystallographic sites in applying onsite energies U_d (Cr 3*d*). In the beginning of the self-consistent cycle, local noncollinear magnetic fields were applied at the Cr sites with dominant components along the *c* and four times weaker fields along the *a* axis in order to break spin symmetry and allow possible canted antiferromagnetic ground states to emerge. This alignment of spin favors a spin structure as predicted by muon spin relaxation [15] but does not enforce it. Spin density waves predicted to be present in β-$CaCr_2O_4$ by Sugiyama *et al.* [14] were not considered for the calculation. Experimental low-temperature lattice constants extracted from the

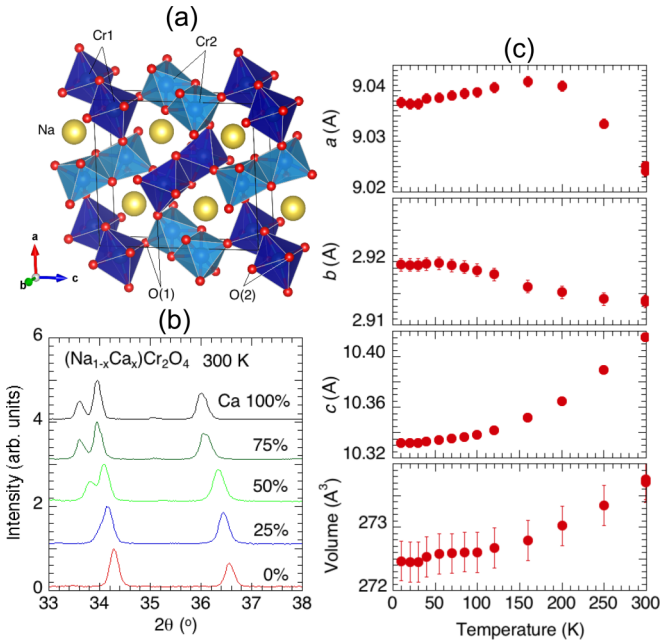

FIG. 1. Temperature dependence of x-ray diffraction patterns for $(Na_{1-x}Ca_x)Cr_2O_4$. (a) Schematic view of the crystal structure [2,24]. (b) Ca-doping dependence of the XRD patterns of $NaCr_2O_4$: expanded view of the XRD patterns in the angle range from 33° to 38°. (c) Temperature dependence of the lattice constants for $NaCr_2O_4$.

present XRD data of both compounds were used to calculate the density of states. Fractional coordinates for both compounds are identical and the positions of $NaCr_2O_4$ according to Sakurai *et al.* [1] were used in the calculation.

III. EXPERIMENTAL RESULTS

A. X-ray diffraction

Temperature dependence of x-ray diffraction (XRD) patterns were measured for $(Na_{1-x}Ca_x)Cr_2O_4$ ($x = 0$, 0.25, 0.5, 0.75, and 1.0) in the the 2θ-angle range from 30° to 80° [16]. Examples of the expanded view in the angle range from 33° to 38° of the XRD patterns are shown in Fig. 1(b). Figure 1(c) shows the temperature dependence of the lattice constants and volume for $NaCr_2O_4$.

The structure was analyzed with RIETAN-FP and example fits are shown in the Supplemental Material [23]. We successfully plotted the all data of the temperature dependence of the XRD patterns of $NaCr_2O_4$ with the same crystal symmetry of *Pnma*. The XRD shows a monotonic decrease of the unit-cell volume as shown in Fig. 1(c) while decreasing temperature down to 10 K with a total volume reduction of about 0.46% between 300 and 10 K. Our present results agree with the previous measurements by Sugiyama *et al.* for $NaCr_2O_4$ at 1.7 K and for $Ca_{0.15}Na_{0.85}Cr_2O_4$ at 1.6 K [14]. Interestingly, the lattice constant along the *a* axis increases down to about 200 K and decreases gradually below 200 K; that along the *b* axis increases down to 70–80 K and the change in the lattice constant of *b* is little below 70 K; while that along the *c* axis decreases monotonically. The results show that the compressibility along the *c* axis is larger than that of the *ab* plane. The temperature-induced changes of the lattice constants of $NaCr_2O_4$ are in contrast to those of NaV_2O_4 [9]. In NaV_2O_4 the *a* and *b* axes decreased monotonically with decreasing the temperature and the change in the lattice constant of *c* is small and slightly increased at low temperature [25]. Thus, in $NaCr_2O_4$ the crystal is compressed along the *c* axis, while the compressibility becomes small below around T_N. In both $NaCr_2O_4$ and NaV_2O_4 the gap becomes wider with decreasing the temperature. On the other hand, in $NaCr_2O_4$, Ca substitution induced the increase of the lattice parameters, indicating negative pressure effect.

The diffraction of $NaCr_2O_4$ seemingly develops an additional peak 34.6° with decreasing temperature [see Fig. S2(b) in the Supplemental Material [16]]. The additional peak is located on the higher-angle side of the main peak at 34.3°. We assign the additional peak to the (302) reflection and the main peak to the (004) reflection. Due to the unusual temperature dependence of the lattice constants, the peaks are merged at higher temperatures and split at lower temperatures. Model curves based on the Rietvelt analysis are added to the plot to demonstrate the validity of the peak assignment. Similar temperature-induced peak splittings are observed around higher angles of 51°, 61.5°, and 63.5° at lower temperature [Fig. S2(a) [16]]. A similar peak separation can be observed in $Na_{0.75}Ca_{0.25}Cr_2O_4$ below 40 K [Fig. S2(c) [16]]. The lattice constants of *a* and *b* change inversely to that of *c* and thus above peak separation occur at low temperatures at $x = 0$ and 0.25 samples. Corresponding peaks for the $x = 0.5$, 0.75, and 1.0 samples are observed already at room temperature. At $x < 0.25$ the lattice constants change as shown in Fig. 1(c), while at $x > 0.5$ the lattice constants of *a*, *b*, and *c* decrease monotonically with decreasing the temperature and those of *a* and *b* increase at low temperatures [26].

The Ca substitution causes an increase of the lattice constants as shown in Fig. 1(c): the change in the *c* axis was on the order of 0.2 Å at 300 K which was much larger compared to those of the order of 0.06 Å for the *a* axis and 0.02 Å for the *b* axis at the Ca-end compound [1]. The order of these changes at 10 K was the same as those at 300 K, while the lattice constant along the *c* axis at 10 K did not show a remarkable *x* dependence. Thus, the Ca substitution mainly caused the elongation along the *c* axis.

No temperature-induced structural transition was observed. Also, Ca substitution changes only the lattice parameters, and not the fractional coordinates of the atoms. Thus, the large changes in electronic properties induced by the Ca substitution are more likely related to the electron doping effect than structural triggers.

B. Photoelectron spectroscopy: Temperature dependence

Figure 2(a) shows Ca-concentration dependence of the valence band spectra at $h\nu = 40$ eV and 300 K. The intensity is normalized by the area measured. We also measured the core-level spectra of Na 2*p* and confirmed that there is no charge up of the samples [16].

In Fig. 2(b), an expanded view of Fig. 2(a) near E_F is shown. The intensity at the binding energy of $E_b = 1.5$ and ~4 eV increases at $h\nu = 85$ eV (not shown here), where E_b is the electron binding energy. The ionization cross section of Cr 3*d* is much higher than that of O 2*p* at $h\nu = 85$ eV [27].

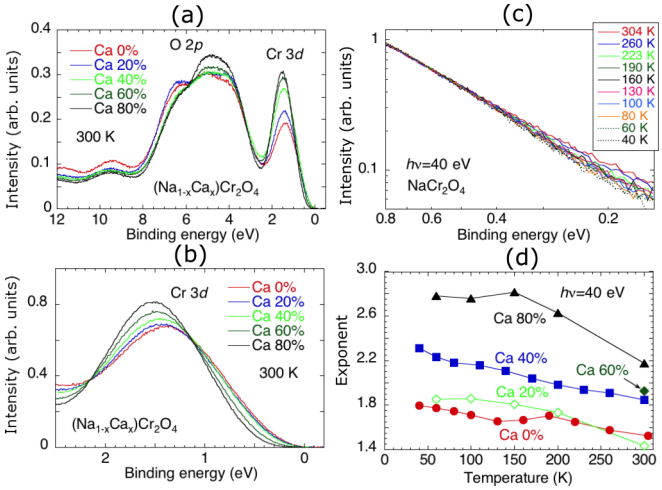

FIG. 2. (a) Ca-concentration dependence of the valence band spectra for $(Na_{1-x}Ca_x)Cr_2O_4$. (b) Expanded view of the valence band spectra near the Fermi edge. (c) The valence band spectra near the Fermi level in a log-log scale for $NaCr_2O_4$. (d) Temperature dependencies of the exponents for $(Na_{1-x}Ca_x)Cr_2O_4$, assuming a power-law behavior of the intensity of the valence band spectra near the Fermi level.

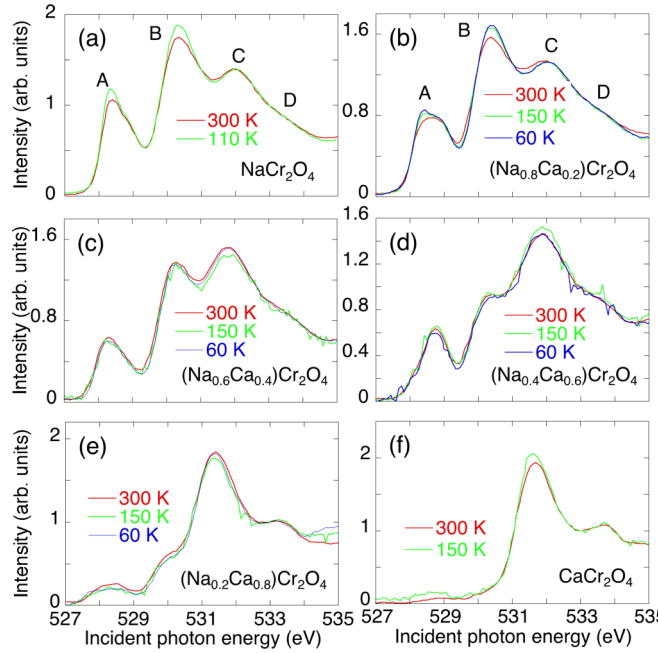

FIG. 3. (a)–(f) Ca concentration and temperature dependence of the x-ray absorption spectra at the O K-absorption edge for $(Na_{1-x}Ca_x)Cr_2O_4$ without magnetic field. The intensity is normalized by the intensity at 533 eV.

Therefore, the increase of the intensity of $E_b = 1.5$ and ~4 eV at $h\nu = 85$ eV is likely originated from Cr 3d. We found the opening of the gap at the Fermi level (E_F) and the increase of the Cr 3d DOS with increasing the Ca concentration as shown in Fig. 2(b).

Figure 2(c) shows the valence band spectra near E_F in a log-log scale for $NaCr_2O_4$. The data show a good power-law behavior in the energy range at $E_b < 0.5$ eV. We approximate the intensity with an exponent function to discuss the the gap around E_F through the change in the exponent α, assuming a power-law behavior $I \sim {E_b}^{\alpha}$ for simplicity, where I and E_b are the intensity and the electron binding energy, respectively [9,28]. As the exponent is larger, the spectral weight at E_F becomes smaller. We assume that the reduction of the spectral weight at E_F corresponds to the enhanced electrical resistivity. Figure 2(d) shows the temperature dependence of the exponents (α). The results indicate that both the Ca substitution and the decrease of the temperature lead to an insulating state. The electronic structure of $NaCr_2O_4$ near the Fermi level is very similar to that of NaV_2O_4 [9]. However, NaV_2O_4 showed metallic character down to 40 mK. The main difference between $NaCr_2O_4$ and NaV_2O_4 is observed in the exponent described above; in NaV_2O_4 it ranges from 0.65 to 0.9, while in $NaCr_2O_4$ it ranges from 1.5 to 1.8. A larger exponent makes $NaCr_2O_4$ more insulatorlike at low temperatures.

The resistivity obeyed Arrhenius-type temperature dependence with the energy gap of 115 meV above T_N and 47 meV below T_N [1,29,30]. The energy gap estimated from the resistivity indeed drops significantly when magnetic field is applied [1,29]. On the other hand, the actual electrical resistivity keeps increasing with decreasing the temperature even under magnetic field. This is simply due to the decrease of the number of thermally activated carrier electrons at low temperatures. In our PES the gap at E_F is not clear because the DOS near E_F decreases constantly with decreasing E_b as described above. However, the relative change in the values of the exponent in Fig. 2(d) as a function of x correspond well to the slope of the logarithm of the resistivity [16]. This indicates that the spectral intensity at the Fermi level decreases with decreasing temperature, corresponding to the increase of the electrical resistivity as temperature decreases [see Figs. S1(a) and S1(b) [16]]. We should note that $NaCr_2O_4$ showed thermally activated conductivity with changing the energy gap at T_N while $Na_{0.5}Ca_{0.5}Cr_2O_4$ showed two-dimensional variable range hopping [29,30]. It seems that the exponent for $NaCr_2O_4$ changes its temperature dependence around T_N in Fig. 2(d).

On the other hand, as the Ca concentration increases the electrical resistivity increases [see Figs. S1(a) and S1(b) [16]], corresponding to the increase of the actual energy gap at the Fermi level as described below. This is consistent with suppressed spectral intensity near the Fermi level [Fig. 2(d)] and larger exponent [Fig. 2(d)] as the Ca concentration increases.

C. X-ray absorption spectroscopy

We performed the XAS study with total electron yield mode at the O K- and Cr L_3-absorption edges [16]. Ca-concentration dependence of the spectra at the O K-absorption edges are shown in Figs. 3(a)–3(f), where the main peaks are labeled from A to D without magnetic field. The intensity is normalized by the intensity at 533 eV. Note that we also show a case when the intensity is normalized by the area in the energy range from 527 to 535 eV for comparison in the Supplemental Material [16]. The spectra at the O K-absorption edge show that there are little temperature dependencies. Those at the Cr L_3-absorption edge show nearly no temperature

dependence [16]. These spectra are very similar to those measured by Okamoto *et al.* at room temperature [11].

The band calculations also showed that the first peak A is attributed to the unoccupied part of the Cr 3*d* $t_{2g\uparrow}$ band and the second prominent peak including B, C, and D to remaining unoccupied Cr 3*d* $t_{2g\downarrow}$, $e_{g\uparrow}$, and $e_{g\downarrow}$ bands [24]. The Anderson impurity model calculations showed that $NaCr_2O_4$ is in the mixed valence state of Cr^{3+} and Cr^{4+} and the charge state of Cr in $CaCr_2O_4$ may be in the Cr^{3+} state, where Cr 3*d* states mix strongly with the O 2*p* state [12]. The theory also suggested that the peaks A and B correspond to the components of Cr^{4+} and the peak C dose the that of Cr^{3+}.

Figures 3(a) and 3(b) show a slight increase of the intensity of the peaks A and B in $NaCr_2O_4$ and $Na_{0.8}Ca_{0.2}Cr_2O_4$ at low temperatures. In $CaCr_2O_4$ in Fig. 3(f) we observe the increase of the peak intensity around 531.5 eV and that at the energy less than 529 eV. The peak A also shows a slight shift of the peak to lower energy at 110 K in $NaCr_2O_4$, and this is more clearly observed in $(Na_{0.8}Ca_{0.2})Cr_2O_4$. The Arrhenius plot of the temperature dependence of the resistivity indicates a smaller gap below T_N and the resistivity increases at low temperatures. The decrease of the thermally excited carriers at low temperatures may enhance the unoccupied t_{2g} and e_g states, leading to the slight increase of the peaks A and B in the absorption spectra. It is also likely that the thermal broadening is reduced at low temperatures. On the other hand, the theory suggested that the peaks A and B correspond to the components of Cr^{4+} and the ground state of Cr^{4+} mainly consists of $3d3\underline{L}$, where $\underline{L}$ is the ligand hole of oxygen [12]. The O 1*s* electron exited to the ligand state in the O *K*-absorption spectra. Therefore, the increase of the intensity of the peaks A and B also indicates the increase of the oxygen holes at low temperatures.

Figures 3(c)–3(f) do not show significant temperature dependence for the samples with the Ca content more than 40%. The transport properties indicate antiferromagnetic order in $NaCr_2O_4$ and $Na_{0.8}Ca_{0.2}Cr_2O_4$, while the other samples do not show such magnetic order except $CaCr_2O_4$ [1,16,26]. The increase of the hybridization at low temperatures in $NaCr_2O_4$ and $Na_{0.8}Ca_{0.2}Cr_2O_4$ corresponds to the magnetic order and thus this temperature-induced change in the electronic structure may correlate to the magnetic order. This observation suggests that the evolution of long-range magnetic order in $Na_{1-x}Ca_xCr_2O_4$ enhances the *p*-*d* hybridization. This is likely to be relevant to the decrease of the gap below T_N, suggested from the transport measurements [29,30]. Detailed study of the temperature dependence of the electronic structure with high-resolution angle-resolved PES remains as a future challenge to understand the correlation between the electronic structure and the long-range magnetic order.

On the other hand, the Ca substitution causes remarkable changes in the both O *K*- and Cr L_3-absorption spectra. The intensity of the peaks A and B decreases gradually. These peaks correspond to the hybridizations between O 2*p* and Cr 3*d*. Thus, the Ca substitution decreases the hybridization between O 2*p* and Cr 3*d* and increases that between O 2*p* and Na 3*p* and that between O 2*p* and Cr 4*s*, 4*p*, making the system insulator. The Cr spectra show the spin-orbit splitting of $2p_{1/2}$ and $2p_{3/2}$ and complex structure [31,32]. The electronic structure of Cr in the Ca 100% sample is very similar to that of

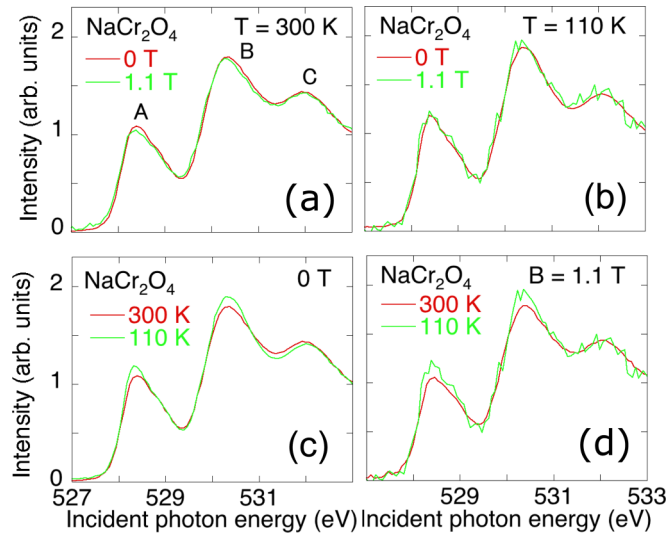

FIG. 4. X-ray absorption spectra at the O *K*-absorption edge for $NaCr_2O_4$. (a) The spectra at 0 and 1.1 T at 300 K. (b) The spectra at 0 and 1.1 T at 110 K. (c) The spectra at 110 and 300 K at 0 T. The data in (c) are the same as those in Fig. 3(a). (d) The spectra at 110 and 300 K at 1.1 T.

Cr_2O_3 [16], indicating the Cr^{3+} charge state of the Ca 100% sample [31].

Nuclear magnetic resonance study of $NaCr_2O_4$ showed a single peak at the frequency between the CrO_2 and Cr_2O_3, also indicating the mixed Cr valence [10]. But, it is noted that the Cr electronic state of CrO_2 is under debate [33,34]. The NMR spectra of CrO_2 always showed two peaks. One possible origin is the electronic phase separation which may be induced in the double-exchange systems [33], another is the charge fluctuation of $Cr^{+4\pm1/3}$, which is a likely origin of the metallic ferromagnetism in CrO_2 [34]. Korotin *et al.* theoretically considered that CrO_2 is a negative charge transfer gap material and both localized and itinerant *d* electrons exist, resulting in the ferromagnetic order due to the double exchange [35,36]. This situation of CrO_2 is very similar to those of $NaCr_2O_4$ suggested by the DFT calculations [24]. In CrO_2 they showed that O 2*p* band extended over to E_F, hybridized with Cr 3*d*, and crossed E_F around the Γ point, making CrO_2 metallic. This could be described with the Zaanen-Sawatzky-Allen (ZSA) diagram [37].

We also measured the XAS spectra of the Ca 0%, 15%, and 40% samples at the O *K*-absorption edge under the magnetic field of 1.1 T at 300 and 110 K [16]. Both temperature and magnetic field did not show significant effect for the Ca 15% and 40% samples [16]. The results of the Ca 0% sample are shown in Figs. 4(a)–4(d). In $NaCr_2O_4$ there is almost no effect of the magnetic field at 300 and 100 K as shown in Figs. 4(a) and 4(b), while the temperature enhances the intensity of the peaks A and B at 110 K slightly as shown in Figs. 4(c) and 4(d). Contrastingly, the Ca substitution causes the significant decrease of the absolute intensity of peaks A and B and the system becomes insulator. These changes in the electronic structures induced by the Ca substitution correspond well to the results of the resistivity measurements.

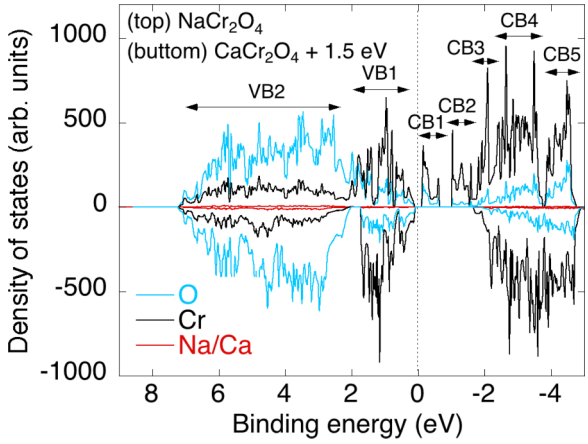

FIG. 5. Comparison the density of states of the low-temperature phases of $NaCr_2O_4$ (top) and $CaCr_2O_4$ (bottom). Valence and conduction bands are divided into two (VB1 and VB2) and five parts (CB1–CB5) for convenience, respectively.

The energy levels of t_{2g} and e_g states may change under the magnetic field, resulting in the broadening of the width of the spectra. On the other hand, theory suggested that the thermal effects broaden the t_{2g} and e_g states with the final-state vibrational broadening [38]. Thus, the thermal or vibrational effect could compensate the magnetic field effect at low temperatures. Another possible reason is the insensitivity to the magnetic field of the spectra that the magnetic field of 1 T is too weak to observe the broadening of the spectra with the present spectral resolution.

Finally, we add a fact that magnet polarization dependence of the XAS spectra at O K edge at 300 K did not show any difference because this system is in the paramagnetic state [16]. This indicates the reliability of the XAS measurements.

IV. DFT CALCULATIONS

We performed DFT calculations for $NaCr_2O_4$ and $CaCr_2O_4$ to compare with our experimental results. The calculated density of states (DOS) of $NaCr_2O_4$ with a Cr onsite energy $U_d = 4$ eV is shown in the upper part of Fig. 5. The valence band is divided into two main contributions we will refer to as VB2 with O $2p$ dominance and VB1 closer to the Fermi level with Cr $3d$ derived states dominating, but still significant O $2p$ contribution. The conduction band hosts a number of localized bands. CB1 just above the Fermi level with a similar ratio of Cr $3d$ and O $2p$ states as VB1. CB2 at around 1.5 eV above the Fermi level with almost pure Cr $3d$ character followed by a quasicontinuum of states: CB3 at 2 eV, CB4 around 3 eV, and CB5 at 4.5 eV, each with increasing O $2p$ contribution. At even higher energies, a low-density continuum of states exists with Na, Cr, and O character. Compared to previous published calculations of $NaCr_2O_4$ using $U_d = 3$ eV within the fully localized limit [24], the present DOS exhibits a clear gap at the Fermi level and a well-separated CB2 located closer to the Fermi level.

It should be noted that DFT is not able to reproduce the effects of the charge transfer energy Δ as proposed in the ZSA scheme [37]. The charge transfer is linked to the hybridization between Cr d and O p orbitals so we chose to include an analysis of O p onsite energies U_p on the electronic properties in conjunction with the application of Cr d energies U_d. However, no significant changes to the electronic nor the magnetic structure were induced by varying U_p and, hence, further discussion of its effects was omitted from this paper [16].

TABLE I. Gap size of $NaCr_2O_4$ in eV as a function of onsite energies U_d. Negative values indicate a band overlap at the Fermi level.

	$U_d = 0$ eV	2 eV	4 eV
Gap (eV)	−0.02	0.06	0.20

A. Onsite energy U_d in $NaCr_2O_4$

In $NaCr_2O_4$ a transition from a semimetallic (or zero-gap) to a semiconducting state is triggered by the addition of onsite energies at the Cr sites (U_d). The gap size as a function of this parameter was estimated from the leading edge of the calculated DOS and is shown in Table I. A negative gap value indicates a semimetallic state, i.e., an overlap of conduction band minimum and valence band maximum. In tendency, adding U_d indeed decreases the band overlap and can trigger a gap opening at the Fermi level between the heavily Cr d and O p hybridized VB1 and CB1. This result diverges from the predicted phase diagram of U_d vs Δ by Taguchi *et al.* [12] as the present DFT predicts an MIT as a function of U_d alone without the need to incorporate Δ. The DFT calculations predict the presence of spin disproportionation between Cr1 and Cr2 (shown in Table II). A low- and high-spin site exist in the magnetic ground state for all choices of onsite energies. In order to highlight the difference in moment between the Cr sites, the table shows the total magnetic moment of the low-spin site and the difference in moment between the low- and high-spin sites. Interestingly, the increase of U_d leads to a state of increased spin disproportionation. While in its semimetallic state ($U_d = 0$ eV), the moment of both Cr sites differs by less than 3% of their total magnitude. The disproportionation increases to 18% for $U_d = 4$ eV. This is mainly due to the reduction of the moment on the low-spin site ($-0.28\,\mu_B$/4 eV), while the moment at the high-spin site only slightly increases ($+0.06\,\mu_B$/4 eV). Nozaki *et al.* determined the magnetic moment of Cr in $NaCr_2O_4$ as $\mu = 2.39 \pm 0.10\,\mu_B$ using μ-spin rotation [15]. The authors mention, however, that a detailed determination of the spin structure is not possible due to the single lattice site which is theoretically predicted to be the only place probed by the muons. The spin disproportionation

TABLE II. Magnetic moment on the low-spin Cr site/difference in magnetic moment (spin disproportionation) to the high-spin Cr site of $NaCr_2O_4$ in μ_B as a function of onsite energies U_d.

	$U_d = 0$ eV	2 eV	4 eV
Moment (μ_B)/ difference (μ_B)	2.18/+0.06	2.07/+0.17	1.90/+0.35

predicted by the present calculations can therefore not be validated by such measurements. Finally, the DFT does not predict any notable charge disproportionation (not shown) within the muffin-tin radii of the two sites, regardless of onsite energies. This is in agreement with XAS model analysis [12] which predicts a single charge state of both Cr sites, with valence differing only between the Cr in Na and Cr in Ca based compounds.

Considering the transport properties of $NaCr_2O_4$ [16], the following discussions will use $U_d = 4$ eV as onsite energy, in order to capture the insulating, i.e., gapped nature of the material.

B. Comparing $NaCr_2O_4$ with $CaCr_2O_4$

Here we compare the two mother compounds $NaCr_2O_4$ and β-$CaCr_2O_4$ directly with each other. In Fig. 5 we show the density of states of both materials using the same onsite energies ($U_d = 4$ eV) and their respective low-temperature lattice constants. The Fermi level of both compounds is located inside a band gap, but the level of the Ca compound is located close to the conduction band minimum [16], leading to a significant offset between the two DOS. For comparison and as a guide to the eye, we offset the β-$CaCr_2O_4$ by -1.5 eV. This moves the apparent Fermi level from the vicinity of the conduction band towards the valence band maximum, retaining its position inside the gap. This treatment should allow for a more straightforward comparison of the conduction band states with PES and XAS.

Looking at Fig. 5, a couple of differences between both compounds are visible. The gap in β-$CaCr_2O_4$ is with 1.6 eV much larger, compared to the 0.2 eV in $NaCr_2O_4$. Furthermore, the DOS of β-$CaCr_2O_4$ seems to be missing the conduction states related to CB1 and CB2 found in the Na based compound. Finally, the higher-lying conduction states CB3–CB5 are pushed to higher energies (with respect to the valence band maximum).

Figure 6 shows the electron charge-doped DOS calculations of $NaCr_2O_4$ with adding a maximum of four electrons (corresponding to complete substitution of Na with Ca) to the unit cell [39]. This leads to a fully occupied CB1 and indeed pushes CB2 towards higher binding energies closer to the CB3–CB5 continuum. The electron-doped $NaCr_2O_4$ DOS resembles the β-$CaCr_2O_4$ DOS strongly. Furthermore, the spin disproportionation of Cr1 and Cr2 found in the undoped system is removed, making the magnetic properties resemble that of β-$CaCr_2O_4$ as well.

The electron doping could be the source of the Ca-concentration-dependent shift of the 1.5-eV peak seen in the PES of Fig. 2 as additional states are transferred from CB1 to energies below the Fermi level. CB1 transferring states into the VB1 would also explain the reduction of peak A's intensity in the O K-edge XAS in Fig. 3. Thus, the DFT calculations show the unoccupied t_{2g} and e_g states disappearing upon the Ca doping in agreement with the O K-edge interpretation.

CB2 moving to higher binding energies would lead to the transfer of peak B's weight in the O-edge XAS towards higher photon energies. Indeed, we may attribute the increased prominence of peak C in the O-edge XAS to CB2 states being pushed towards higher binding energies. It should be noted

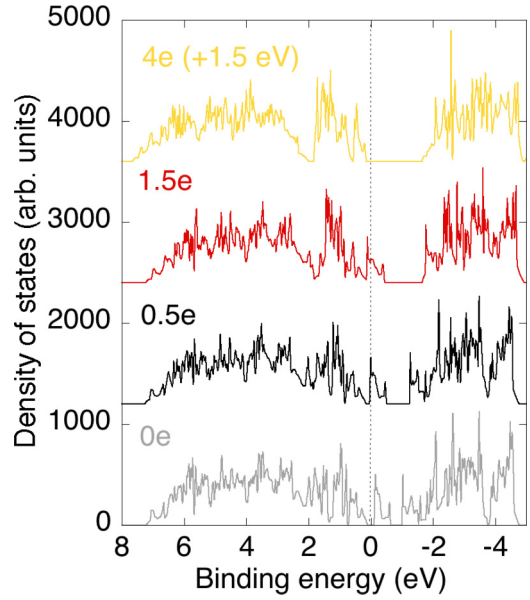

FIG. 6. The evolution of the $NaCr_2O_4$ total DOS as a function of electron doping in the unit cell. The doping predicts a transition from zero gap to semimetal to insulating behavior.

though that the DOS predicts CB2 to be almost entirely dominated by its Cr 3d character, which should make its sensitivity to the O-edge XAS much lower compared to the other conduction bands. Looking at the Cr-edge XAS the lower photon energy peaks G and H actually increase in intensity upon Ca substitution (see the Supplemental Material [16]) giving an inverted scenario to the O edge. The increase in the Cr-edge spectra intensity is completely opposed to the DFT calculation results. As a ground-state calculation, the predictability of DFT is naturally limited when it comes to final-state dominated XAS spectra like the Cr 2p-3d transition. The O-edge XAS, on the other hand, is much more dominated by the ground state than complex final-state satellite structure and the good match between DOS and O-edge XAS supports this notion. Note that the 3d orbital in Cr is more localized as compared with the O 2p state, thus, the many-body picture is required to describe the Cr 3d state and the electrons in O 2p orbital are delocalized (one-electron picture is valid). The O 2p XAS spectra may have an excitonic contribution to a certain degree because the final state has a 1s core hole [40,41]. This effect may be small in the spectra at O K-absorption edge (compared to Cr L) because of the small number of O 2p holes [42–44]. This is supported by the fact that XAS calculations showed that the effect of the O 1s core hole in transition metal oxides on the band structure was weak [45,46].

In a previous study [12], the Cr-edge XAS spectra of both compounds (Na and Ca) were fitted to models using final-state effects and a good match between theory and experiment was found. While the energies extracted from such calculations (like the charge transfer Δ, for example) cannot be directly used to feed DFT calculations, one may still investigate the influence of onsite energies based on ground-state properties alone and compare $NaCr_2O_4$ to $CaCr_2O_4$ with each other. In the following, we are going to investigate the overall phase diagram of onsite energies of $CaCr_2O_4$.

TABLE III. Gap size of β-$CaCr_2O_4$ in eV as a function of onsite energy U_d.

	$U_d = 0$ eV	2 eV	4 eV
Gap (eV)	0.73	1.24	1.67

C. Onsite energy U_d in $CaCr_2O_4$

As with $NaCr_2O_4$, we compare the influence of U_d on the electronic and magnetic properties in $CaCr_2O_4$. Table III summarizes the gap sizes as a function of onsite energies U_d. β-$CaCr_2O_4$ has a fully gapped band structure for all onsite energies.

In Table IV the magnetic moment of the low-spin site and the difference in moment between low- and high-spin sites is shown for β-$CaCr_2O_4$. The magnetic moment is almost constant, changing at most 0.08 μ_B across the whole phase diagram. The two Cr sites are essentially identical in their spin state, differing at most 1% of their magnetic moment. The stability of magnetic moment is most likely related to the fully occupied Cr states (VB1 and CB1 in $NaCr_2O_4$ becoming VB1 in $CaCr_2O_4$). The higher total moment compared to $NaCr_2O_4$ is accompanied by a lower Cr valency in $CaCr_2O_4$. As compared to $NaCr_2O_4$, the Cr moment within the muffin-tin sphere is reduced by $\approx 0.1e$ for the low-spin site regardless of onsite energies and between $\approx 0.1e$ ($U_d = 0$ eV) and $\approx 0.05e$ ($U_d = 4$ eV) for the high-spin site. The presence of spin degeneracy, as opposed to the spin disproportionation in $NaCr_2O_4$, may be related to the larger spatial extension and therefore hybridization of the Ca $3p$ orbitals vs that of the Na $2p$ orbitals or the difference in available spin configurations in the valence bands of both compounds. The previous electron-doped calculations of $NaCr_2O_4$, however, suggest that the electron doping alone is responsible for destroying the spin disproportionation. Without applying more advanced analysis of the charge distribution, it is not possible to comment on the absolute valency of either Cr or O based on the DFT, however, the strong hybridization of Cr and O in both valence and conduction bands would suggest that a purely ionic picture is not a suitable description for either system. This is supported by the strong mixing of the ground-state configurations (d^nL^m) derived from XAS [12] where both Na and Ca compounds are shown to mix mainly two (albeit different) ionic ground-state configurations for a correct theoretical description of the adsorption spectra. The predicted moment at the Cr site matches reasonably well the $\mu = 2.39 \pm 0.10\ \mu_B$ extracted from μ-spin rotation [14], but even though the gap is well established in the present compound, we caution a quantitative comparison without an advanced charge analysis as mentioned above in the case of the Na-based compound.

TABLE IV. Magnetic moment on the low-spin Cr site/difference in magnetic moment (spin disproportionation) to the high-spin Cr site of β-$CaCr_2O_4$ in μ_B as a function of onsite energy U_d.

	$U_d = 0$ eV	2 eV	4 eV
moment (μ_B)/ difference (μ_B)	2.50/+0.02	2.46/+0.01	2.42/+0.01

V. DISCUSSION

The Ca substitution is the most effective to change the electronic structure as shown in Fig. 3. The Ca substitution induced negative pressure effect: the increase of the lattice parameters especially along the c axis on the order of $\sim$0.2 Å with decreasing the hybridization between Cr d and O $2p$ [1]. Therefore, it is reasonable to consider that the Ca substitution also caused the decrease of the O $2p$–Cr $3d$ hybridization because the increase of the atomic distances. Lattice expansion may cause the narrowing of the bandwidth as observed in the change in the valence band spectra and thus the system may have a possibility to be an insulator at the Ca-rich side. Actually, the Ca substitution caused the narrowing of the $3d$ DOS around $E_b = 1.5$ eV and changed the Cr valence from the mixed valence to 3+ as shown in Fig. 2(b), resulting in the decrease of the p-d hybridization and the band gap at the Fermi level wider. The conduction band above the Fermi level (the peaks A and B) were weakened by the Ca substitution as shown in Fig. 3. The decrease of the DOS of the peak A affects the DOS at the Fermi level because the tail part of the DOS above the Fermi level may be extended to the Fermi level, resulting in the insulating state.

Using the DFT calculations, we investigated the Ca-substitution effect to the band structure of $NaCr_2O_4$ from the point of the crystal structure change alone. We find that the DOS of $NaCr_2O_4$ using the structure of β-$CaCr_2O_4$ is essentially identical to that of $NaCr_2O_4$, confirming that the lattice modification has little to no influence on the electronic properties upon Ca substitution [16]. Hence, the DFT calculations suggest that the electron doping by the Ca substitution is the main driving force to modify the electronic and magnetic properties of the solid solution and that the influence of the structural degrees of freedom may be ignored compared to that of the electron doping. The DFT calculations show that the Ca substitution weakened the intensity of the conduction bands of CB1 and CB2 just above the Fermi level as shown in Fig. 6. Thus, the electron doping into $NaCr_2O_4$ can cause a modification in the band structure, where the hybridized DOS just above and below E_F are merged into the conduction and valence bands, respectively, which causes the widening of the gap, leading the system to more insulating.

On the other hand, in $NaCr_2O_4$ the temperature dependence of the crystal structure is not simple; the decrease of the temperature-induced compression along the c axis on the order of $\sim$0.1 Å and expansion of the ab plane. Toriyama *et al.* showed that the peak A of the XAS spectra at the O K-absorption edge is mainly due to the hybridization between O(1) $2p_z$ and Cr1 $3d_{yz-xz}$ and Cr2 $3d_{yz\pm xz}$ [24]. One can expect the decrease of the hybridization to open the gap at low temperatures, while the XAS spectra at the O K-absorption edge does not show a significant temperature dependence at zero magnetic field. Thus, the electronic structure above the Fermi level is insensitive to the change in the temperature. Experimentally, temperature dependence of the $3d$ DOS around $E_b = 1.5$ eV is small, but the decrease of the temperature induced the larger exponent as shown in Fig. 2, resulting in the

wider gap. This can be attributed to the temperature-induced shrink of the lattice constant along the c axis. The most striking difference of the electronic structure is that the full substitution of Ca resulted in a loss of the conduction band just above the Fermi level (the peak A of the XAS spectra at the O K-absorption edge), which may affect the DOS at the Fermi level. Thus, the mechanism of the gap opening with the Ca substitution is different from that with the temperature. Temperature induces only a slight change in the electronic structure of the valence and conduction bands in $NaCr_2O_4$.

The Cr $3d$ band hybridized strongly with the O $2p$ band and thus the ligand hole states are possibly formed in the O $2p$ site because it decreases the total energy normally. In negative-Δ insulator p-derived DOS should appear near E_F and p-p gap determined by the p-d hybridization strength may be formed. The XAS spectra at O K edge showed the increase of the intensity of the peak A in the Na-rich side, indicating the stronger p-d hybridization. The Anderson impurity model calculations taking into account the negative charge transfer reproduced well the XAS spectra measured at the O K-absorption edge as described above [12]. The DFT calculation indicates the O $2p$ and Cr $3d$ bands spread across the Fermi level as shown in Fig. 5, suggesting a possible p-d hybridization near E_F. The presence of such strong hybridization may suggest a need of the O–Cr bonds and not only the Cr–Cr bonds for a proper description of transport and gap size. The present DFT calculations reproduce the insulating state of the material with onsite energies alone, however, it does not follow that a possible nonzero charge transfer energy may not also play a role in the description of the system in a scenario where a smaller U_d together with a nonzero Δ reproduce a similar gap size.

VI. CONCLUSION

The XRD results indicated no temperature-induced structural transition and, therefore, the anomaly of the magnetoresistivity of $NaCr_2O_4$ at low temperatures is not originated by the structural transition. Our PES showed directly that the decrease of the temperature and the Ca substitution to Na site induced the gradual gap opening.

The magnetic field of 1.1 T did not show the significant effect on the XAS spectra of the Ca 0%, 15%, and 40% samples at the O K-absorption edge, while the temperature induced slight increase of the the hybridization between the Cr $3d$ and O $2p$ orbitals at low temperatures for the Ca 0% and 20% samples.

The Ca substitution is the most effective to change the electronic structure. The XAS spectra showed that the Cr $3d$–O $2p$ hybridized state just above the K edge is suppressed by Ca doping. Consistently, the DFT calculation suggested that the electron doping into $NaCr_2O_4$ solely can cause a modification in the band structure, where the hybridized DOS just above and below E_F are merged into the conduction and valence bands, respectively, which causes the widening of the gap, leading the system to more insulating. The mechanism of the gap opening with the Ca substitution is different from that with the temperature. DFT further suggests that electron doping by Ca substitution is the main driving force of the modification of the electronic and magnetic properties of the solid solution and that the influence of structural degrees of freedom may be ignored. The main change in the electronic structure with the Ca doping is not originated by the change in the crystal structure. For $NaCr_2O_4$ and $Na_{0.8}Ca_{0.2}Cr_2O_4$, the O K-edge absorption spectra suggest the increase in the p-d hybridization is relevant to the antiferromagnetic ordering.

ACKNOWLEDGMENTS

The experiments were performed at HiSOR beam lines BL-1, BL-7, and BL-14 at Hiroshima University under Proposals No. 12-A-1, No. 13-A-1, and No. 13-B-1, No. 14-A-4, No. 14-A-5, and No. 14-B-17. We thank the N-BARD, Hiroshima University, for supplying the liquid helium. We thank J. Okamoto at NSRRC in Taiwan for his kindness to send the information about the XAS spectra measured at Photon Factory.

[1] H. Sakurai, T. Kolodiazhnyi, Y. Michiue, E. Takayama-Muromachi, Y. Tanabe, and H. Kikuchi, Unconventional colossal magnetoresistance in sodium chromium oxide with a mixed-valence state, Angew. Chem. Int. Ed. **51**, 6653 (2012).

[2] H. Sakurai, Magnetic and electronic properties of $Ca_{1-x}Na_xCr_2O_4$: Double-exchange interactions and ligand holes, Phys. Rev. B **89**, 024416 (2014).

[3] F. J. Morin, Oxides which Show a Metal-to-Insulator Transition at the Néel temperature, Phys. Rev. Lett. **3**, 34 (1959).

[4] M. Imada, A. Fujimori, and Y. Tokura, Metal-insulator transitions, Rev. Mod. Phys. **70**, 1039 (1998).

[5] C. Weber, D. D. O'Regan, N. D. M. Hine, M. C. Payne, G. Kotliar, and P. B. Littlewood, Vanadium Dioxide: A Peiels-Mott Insulator Stable against Disorder, Phys. Rev. Lett. **108**, 256402 (2012).

[6] K. Hasegawa, M. Isobe, T. Yamauchi, H. Ueda, J. Yamaura, H. Gotou, T. Yagi, H. Sato, and Y. Ueda, Discovery of Ferromagnetic-Half-Metal-to-Insulator Transition in $K_2Cr_8O_{16}$, Phys. Rev. Lett. **103**, 146403 (2009).

[7] A. Nakao, Y. Yamaki, H. Nakao, Y. Murakami, K. Hasegawa, M. Isobe, and Y. Ueda, Observation of structural change in the novel ferromagnetic metal-insulator transition of $K_2Cr_8O_{16}$, J. Phys. Soc. Jpn. **81**, 054710 (2012).

[8] K. Yamaura, M. Arai, A. Sato, A. B. Karki, D. P. Young, R. Movshovich, S. Okamoto, D. Mandrus, and E. Takayama-Muromachi, NaV_2O_4: A quasi-1D Metallic Antiferromagnet with Half-Metallic Chains, Phys. Rev. Lett. **99**, 196601 (2007).

[9] T. Qian, K. Nakayama, Y. Sun, T. Arakane, T. Sato, T. Takahashi, K. Yamaura, and E. Takayama-Muromachi, High-resolution photoemission study of NaV_2O_4, J. Phys. Soc. Jpn. **78**, 024709 (2009).

[10] H. Takeda, Y. Shimizu, and M. Itoh, Magnetic frustration effects in the new colossal magnetoresistance oxide $NaCr_2O_4$, J. Korean Phys. Soc. **62**, 1914 (2013).

[11] J. Okamoto, Y. Takahashi, T. Sudayama, Y. Yamasaki, H. Nakao, H. Sakurai, T.-H. Kao, H.-D. Yang, and Y. Murakami, O 1*s* and Cr 2*p* XAS study of electronic structures of $Na_{1-x}Ca_xCr_2O_4$, (in Japanese) Photon Factory Activity Report 2012 Part B, No. 164.

[12] M. Taguchi, H. Yamaoka, Y. Yamamoto, H. Sakurai, N. Tsujii, M. Sawada, H. Daimon, K. Shimada, and J. Mizuki, Unusual coexistence of negative/positive charge transfer in mixed-valence $Na_xCa_{1-x}Cr_2O_4$, Phys. Rev. B **96**, 245113 (2017).

[13] H. Nozaki, H. Sakurai, M. Harada, Y. Higuchi, J. H. Brewer, E. J. Ansaldo, and J. Sugiyama, Internal magnetic field in the zigzag-chain family (Na, Ca)Cr_2O_4, J. Phys.: Conf. Ser. **551**, 012013 (2014).

[14] J. Sugiyama, H. Nozaki, M. Harada, Y. Higuchi, H. Sakurai, E. J. Ansaldo, J. H. Brewer, L. Keller, V. Pomjakushin, and M. Månsson, Magnetic ground state of novel zigzag chain compounds, $NaCr_2O_4$ and $Ca_{1-x}Na_xCr_2O_4$, determined with muons and neutrons, Phys. Proc. **75**, 868 (2015).

[15] H. Nozaki, H. Sakurai, O. Ofer, E. J. Ansaldo, J. H. Brewer, K. H. Chow, V. Pomjakushin, L. Keller, K. Prša, K. Miwa, M. Månsson, and J. Sugiyama, Magnetic structure for $NaCr_2O_4$ analyzed by neutron diffraction and muon spin-rotation, Phys. B (Amsterdam) **551**, 137 (2017).

[16] See Supplemental Material at http://link.aps.org/supplemental/10.1103/PhysRevB.102.235150 for detail of (i) the temperature dependence of the resistivity and susceptibility, (ii) the temperature dependence of x-ray diffraction patterns for $(Na_{1-x}Ca_x)Cr_2O_4$ ($x = 0$, 0.25, 0.5, 0.75, and 1.0) in the wide-angle range, (iii) Ca concentration and temperature dependence of the valence band and core-level spectra, (iv) Ca concentration, temperature, and magnetic field dependencies of the XAS spectra, (v) magnet polarization dependence of the XAS spectra, (vi) DOS of $CaCr_2O_4$ and its dependence on lattice constants, and (vii) U_p dependence in the DFT caculations are shown, which includes Refs. [1,2,13,47–49].

[17] M. Sawada, K. Yaji, M. Nagira, A. Kimura, H. Namatame, and M. Taniguchi, Design concept and performance of the soft x-ray beamline HiSOR BL14, in *Synchrotron Radiation Instrumentation: Ninth International Conference on Synchrotron Radiation Instrumentation*, edited by J.-Y. Choi and S. Rah, AIP Conference Proceedings Vol. 879 (AIP, Melville, NY, 2007), p. 551.

[18] The ELK FP-LAPW code, Home page: http://elk.sourceforge.net/.

[19] Y. Zhang and W. Yang, Comment on Generalized Gradient Approximation Made Simple, Phys. Rev. Lett. **80**, 890 (1998).

[20] A. G. Petukhov, I. I. Mazin, L. Chioncel, and A. I. Lichtenstein, Correlated metals and the LDA+U method, Phys. Rev. B **67**, 153106 (2003).

[21] A. B. Shick, A. I. Liechtenstein, and W. E. Pickett, Implementation of the LDA + U method using the full-potential linearized augmented plane-wave basis, Phys. Rev. B **60**, 10763 (1999).

[22] F. Bultmark, F. Cricchio, O. Grånäs, and L. Nordström, Multipole decomposition of LDA +U energy and its application to actinide compounds, Phys. Rev. B **80**, 035121 (2009).

[23] F. Izumi and K. Momma, Three-dimensional visualization in powder diffraction, Solid State Phenom. **130**, 15 (2007).

[24] T. Toriyama, T. Konishi, and Y. Ohta, Electronic structure of calcium-ferrite-type cr oxide $NaCr_2O_4$, JPSJ Conf. Proc. **3**, 017003 (2014).

[25] H. Nozaki, J. Sugiyama, M. Månsson, M. Harada, V. Pomjakushin, V. Sikolenko, A. Cervellino, B. Roessli, and H. Sakurai, Incommensurate spin-density-wave order in quasi-one-dimensional metallic antiferromagnet NaV_2O_4, Phys. Rev. B **81**, 100410(R) (2010).

[26] F. Damay, C. Martin, V. Hardy, A. Maignan, G. André, K. Knight, S. R. Giblin, and L. C. Chapon, Zigzag ladders with staggered magnetic chirality in the $S = 3/2$ compound β-$CaCr_2O_4$, Phys. Rev. B **81**, 214405 (2010).

[27] J. J. Yeh and I. Lindau, Atomic subshell photoionization cross sections and asymmetry parameters: $1 \leqslant Z \leqslant 103$, At. Data Nucl. Data Tables **32**, 1 (1985).

[28] J. Voit, One-dimensional Fermi liquids, Rep. Prog. Phys. **58**, 977 (1994).

[29] H. Sakurai, Novel colossal magnetoresistance in $NaCr_2O_4$, J. Korean Phys. Soc. **63**, 583 (2013).

[30] T. Kolodiazhnyi and H. Sakurai, Electronic, thermoelectric, and magneto-dielectric properties of $Ca_{1-x}Na_xCr_2O_4$, J. Appl. Phys. **113**, 224109 (2013).

[31] Yu. S. Dedkov, A. S. Vinogradov, M. Fonin, C. König, D. V. Vyalikh, A. B. Preobrajenski, S. A. Krasnikov, E. Yu. Kleimenov, M. A. Nesterov, U. Rüdiger, S. L. Molodtsov, and G. Güntherodt, Correlations in the electronic structure of half-metallic ferromagnetic CrO_2 films: An x-ray absorption and resonant photoemission spectroscopy study, Phys. Rev. B **72**, 060401(R) (2005).

[32] S. Watanabe, T. Nagasaki, and K. Ogasawara, Relativistic many-electron calculations of $Cr^{3+}L_{2,3}$-edge x ray absorption near-edge structures for Cr^{3+}:α-Al_2O_3 and α-Cr_2O_3 and magnetic circular dichroism of $Cr^{3+}L_{2,3}$-edge x ray absorption near-edge structures for Cr^{3+}:α-Al_2O_3, J. Appl. Phys. **110**, 123524 (2011).

[33] H. Takeda, Y. Shimizu, M. Itoh, M. Isobe, and Y. Ueda, Electronic states of half-metallic chromium oxides probed by ^{53}Cr NMR, J. Phys.: Conf. Ser. **400**, 032098 (2012).

[34] J. H. Shim, S. Lee, J. Dho, and D.-H. Kim, Coexistence of Two Different Cr Ions by Self-doping in Half-Metallic CrO_2 Nanorods, Phys. Rev. Lett. **99**, 057209 (2007).

[35] D. I. Khomskii and G. A. Sawatzky, Interplay between spin, charge, and orbital degree of freedom in magnetic oxides, Solid State Commun. **102**, 87 (1997).

[36] M. A. Korotin, V. I. Anisimov, D. I. Khomskii, and G. A. Sawatzky, CrO_2: A Self-doped Double Exchange Ferromagnet, Phys. Rev. Lett. **80**, 4305 (1998).

[37] J. Zaanenn, G. A. Sawatzky, and J. W. Allen, Band Gaps and Electronic Structure of Transition-metal Compounds, Phys. Rev. Lett. **55**, 418 (1985).

[38] F. M. F. de Groot, J. C. Fuggle, B. T. Thole, and G. A. Sawatzky, $L_{2,3}$ x-ray-absorption edges of d^0 compounds: K^+, Ca^{2+}, Sc^{3+}, and Ti^{4+} in O_h (octahedral) symmetry, Phys. Rev. B **41**, 928 (1990).

[39] The electron charge-doped DOS calculations of $NaCr_2O_4$ in Fig. 6 were performed via the *chgexs* option implemented in the ELK code. Note that the *chgexs* adds mobile carriers (electrons) to the unit cell that can move anywhere as we dope electrons with Ca and to compensate the added charge a positive jellium is added to the unit cell to keep charge neutrality.

[40] F. Frati, Myrtille O. J. Y. Hunault, and Frank M. F. de Groot, Oxygen K-edge x-ray absorption spectra, Chem. Rev. **120**, 4056 (2020).

[41] Y. Liang, J. Vinson, S. Pemmaraju, W. S. Drisdell, E. L. Shirley, and D. Prendergast, Accurate X-Ray Spectral Predictions: An Advanced Self-Consistent-Field Approach Inspired by Many-Body Perturbation Theory, Phys. Rev. Lett. **118**, 096402 (2017).

[42] F. M. F. de Groot, J. Faber, J. J. M. Michiels, M. T. Czyiyk, M. Abbate, and J. C. Fuggle, Oxygen 1s x-ray absorption of tetravalent titanium oxides: A comparison with single-particle calculations, Phys. Rev. B **48**, 2074 (1993).

[43] T. Mizoguchi, I. Tanaka, M. Yoshiya, F. Oba, K. Ogasawara, and H. Adachi, Core-hole effects on theoretical electron-energy-loss near-edge structure and near-edge x-ray absorption fine structure of MgO, Phys. Rev. B **61**, 2180 (2000).

[44] K. Okada and A. Kotani, Oxygen 1s core-level photoemission as a tool to investigate the unoccupied electronic states of cuprates, J. Phys. Soc. Jpn. **75**, 123703 (2006).

[45] E. Z. Kurmaev, R. G. Wilks, A. Moewes, L. D. Finkelstein, S. N. Shamin, and J. Kuneš, Oxygen x-ray emission and absorption spectra as a probe of the electronic structure of strongly correlated oxides, Phys. Rev. B **77**, 165127 (2008).

[46] V. Mauchamp, M. Jaouen, and P. Schattschneider, Core-hole effect in the one-particle approximation revisited from density functional theory, Phys. Rev. B **79**, 235106 (2009).

[47] D. M. Riffe, G. K. Wertheim, and P. H. Citrin, Enhanced Vibrational Broadening of Core-level Photoemission from the Surface of Na(110), Phys. Rev. Lett. **67**, 116 (1991).

[48] L. Lavielle and H. Kessler, Spectrométrie électronique (ESCA) appliquée à la caractérisation de dérivés oxygénés de chrome et de sodium, $Na_xCr_yO_z$, J. Electron Spectrosc. Relat. Phenom. **8**, 95 (1976).

[49] S. Peredkov, G. Öhrwall, J. Schulz, M. Lundwall, T. Rander, A. Lindblad, H. Bergersen, A. Rosso, W. Pokapanich, N. Mårtensson, S. Svensson, S. L. Sorensen, O. Björneholm, and M. Tchaplyguine, Free nanoscale sodium clusters studied by core-level photoelectron spectroscopy, Phys. Rev. B **75**, 235407 (2007).